 CMC, vol.33, no.3, pp.257-273, 2013

Identification of Parameters of a Nonlinear Material Model Considering the Effects of Viscoelasticity and Damage

Jan Heczko[1], **Radek Kottner**[2], **Tomáš Kroupa**[2]

Abstract: This work deals with mechanical properties of a rubber material that is used in modern tram wheels as a damping element. Nonlinear static response as well as strain softening and hysteresis are captured in the material model that is selected. Method of identification of the model's parameters is developed. The identification method relies on successive minimizations with respect to different sets of parameters. Tests in tension, compression and simple shear are performed. Parameters of the material model are identified based on the tension and compression data, while the shear data are used for validation only.

Keywords: Rubber, hyperelasticity, viscoelasticity, Mullins effect, Identification

1 Introduction

Elastomeric materials are nowadays an inherent part of many structures thanks to their (i) ability to reach large deformations without a failure and/or (ii) good vibration damping properties. It is because of the polymeric nature of the materials that these distinctive properties can be achieved. But it is also the main cause of related effects that have to be taken into consideration when modeling the material's response.

An example of an elastomeric part is the utilization of rubber segments in modern tram wheels. Those rubber sprung wheels excel in the reduction of the traffic noise and the rail wear. Innovation of the wheels requires sufficient computational model of the rubber segments considering the segment's complex mechanical behavior.

Among the most noticeable phenomena observable in mechanical behavior of elastomers are: strain induced softening due to miromechanical damage (Mullins effect), hysteresis in the case of cyclic loading and permanent set. Many models and

[1] Department of Mechanics, Faculty of Applied Sciences, University of West Bohemia
[2] European Centre of Excellence, New Technologies for Information Society, Faculty of Applied Sciences, University of West Bohemia

different approaches have been developed over about the past eighty years that focus on description of one particular phenomenon or even a combination of them (typically nonlinear elasticity and some other effect).

The set of models dealing with hyperelasticity seems to be the most extensively elaborated. One large class of hyperelastic material models is based on expressing deformation in terms of strain invariants and is therefore applicable to isotropic materials. These models are for example the neo-Hookean, Mooney-Rivlin, Yeoh and other models, which can be generalized into polynomial form of the first and second strain invariant. The Gent model (see Gent (1996)) also involves a function of the first strain invariant but is not in the polynomial form. Another class of hyperelastic models is based on the micromechanics of molecular chains, this includes the Arruda-Boyce model.

First experimental observation of strain induced softening in filled rubbers can be traced back to Bouasse and Carrière (1903) and Holt (1932). The phenomenon is often referred to as the Mullins effect since he did an extensive experimental and theoretical work on the topic. The influence of stretching on various physical properties of the material is investigated in Mullins (1948) and it is pointed out that properties of unfilled rubbers are significantly less affected by previous stretching than that of filled rubbers. In subsequent works, Mullins and Tobin (1957) and Mullins (1969), for instance, quantitative models have been developed on molecular basis as well as phenomenological ones. Models of stress softening that are widely used in today's computational software were introduced by J. Simo (see e.g. Simo (1987) where also viscoelasticity is considered or Govindjee and Simo (1991) and Govindjee and Simo (1992)). Other well known forms of damage evolution, which result in the strain induced softening, have been proposed by Ogden and Roxburgh (1999) or Qi and Boyce (2004).

Apart from the well known linear theory of viscoelasticity, nonlinear theories have been developed. For example the multiple integral approach or the Shapery model (see e.g. Schapery (1966) or Lévesque, Derrien, Baptiste, and Gilchrist (2008)). A thermodynamically based model with internal variables has been introduced by Simo (1987) and a similar approach is used also in later models (e.g. Bergström and Boyce (1998), Reese and Govindjee (1998))

Objectives of this article:

- Select a constitutive model that is able to capture the effects of nonlinear long-term response, strain induced softening and time-dependence in mechanical behavior of a material.

- Develop a method to identify parameters of the model.

- Apply the method to the rubber of the wheel segments.

2 Material model

2.1 Kinematics

The motion of a body can be described by a mapping $\varphi(\mathbf{X},t) : \Omega_0 \times \mathbb{R} \to \mathbb{R}^3$. Here Ω_0 is the reference configuration of the body and $\mathbf{X} \in \Omega_0 \subset \mathbb{R}^3$ are material coordinates of any particle of the body. Then the deformation gradient $\mathbf{F}$ and its isochoric part $\overline{\mathbf{F}}$ are defined respectively as

$$\mathbf{F}(\mathbf{X},t) := \frac{\partial \varphi}{\partial \mathbf{X}}, \quad \overline{\mathbf{F}} := J^{-1/3}\mathbf{F}, \quad \text{where} \quad J = \det \mathbf{F}, \tag{1}$$

the corresponding right Cauchy-Green strain tensors

$$\mathbf{C} := \mathbf{F}^{\mathrm{T}}\mathbf{F}, \quad \overline{\mathbf{C}} := \overline{\mathbf{F}}^{\mathrm{T}}\overline{\mathbf{F}} = J^{-2/3}\mathbf{C} \tag{2}$$

and the Green-Lagrangian strain tensor $\mathbf{E}$ and its isochoric part $\overline{\mathbf{E}}$

$$\mathbf{E} := \frac{1}{2}\left(\mathbf{C} - \mathbf{I}\right), \quad \overline{\mathbf{E}} := \frac{1}{2}\left(\overline{\mathbf{C}} - \mathbf{I}\right), \tag{3}$$

$\mathbf{I}$ being identity tensor. In the case of incompressible material, which was assumed throughout this work, the strain tensors and their isochoric counterparts coincide.

The eigenvalues of the right Cauchy-Green strain tensor are squares of the principal stretches, λ_1^2, λ_2^2 and λ_3^2.

2.2 Strain induced softening

Mullins effect was captured using the Ogden-Roxburgh model (proposed in Ogden and Roxburgh (1999)) of strain induced softening. One particular advantage from the point of view of parameters identification is that the damage model does not influence the first-loading response. In some other models (Qi-Boyce, Govindjee-Simo), the damage takes place at all times which is for sure physically reasonable but couples the elastic response with the damage evolution. As a consequence, the identification of damage parameters must be carried out together with the identification of the underlying hyperelastic model parameters which is not necessary in the case of Ogden-Roxburgh damage model. Details of this approach are given in section 5.1. The model could be described as follows.

An internal variable η is introduced to quantify the damage at a given material point. The strain energy density function can be written as

$$W = W(\mathbf{F}, \eta). \tag{4}$$

In the case of an isotropic material the strain energy can be expressed as a function of principal stretches λ_1, λ_2 and λ_3. In addition, considering incompressibility

$$\overline{W}(\lambda_1,\lambda_2,\eta) \equiv W(\lambda_1,\lambda_2,(\lambda_1)^{-1}(\lambda_2)^{-1},\eta). \tag{5}$$

The dependency of $\overline{W}(\lambda_1,\lambda_2,\eta)$ on the damage variable η is usually expressed as

$$\overline{W}(\lambda_1,\lambda_2,\eta) = \eta \cdot \tilde{W}(\lambda_1,\lambda_2), \tag{6}$$

where $\tilde{W}(\lambda_1,\lambda_2) = W(\lambda_1,\lambda_2,1)$, which is in fact the strain energy density of a hyperelastic material. The values of η are assumed to lie between 0 and 1.

As a suitable representation of the strain energy density function, the five-parameter Mooney-Rivlin model was chosen in this paper:

$$\begin{aligned} W_{MR}(\lambda_1,\lambda_2,\lambda_3) = {} & C_{10}(I_1-3)+C_{01}(I_2-3)+C_{11}(I_1-3)(I_2-3) \\ & +C_{20}(I_1-3)^2+C_{30}(I_1-3)^3, \end{aligned} \tag{7}$$

where

$$\begin{aligned} & I_1 = \lambda_1^2+\lambda_2^2+\lambda_3^2 \text{ and} \\ & I_2 = \lambda_1^2\lambda_1^2+\lambda_2^2\lambda_3^2+\lambda_1^2\lambda_3^2 \end{aligned} \tag{8}$$

are the first two strain invariants (in terms of principal stretches λ_1, λ_2 and λ_3).

The damage variable η in the Ogden-Roxburgh model is expressed as

$$\eta = 1-\frac{1}{r}\operatorname{erf}\left(\frac{\left(W_m-\tilde{W}(\lambda_1,\lambda_2)\right)}{m-\beta W_m}\right), \tag{9}$$

where r, m and β are parameters of the model, W_m is the maximum strain energy density achieved at the material point during the loading prior to the current time, t,

$$W_m(t) = \max_{\tau\le t}\tilde{W}(\lambda_1(\tau),\lambda_2(\tau)), \tag{10}$$

and the *error function* is defined as

$$\operatorname{erf}(z) := \frac{2}{\sqrt{\pi}}\int_{t=0}^{z} e^{-t^2}\mathrm{d}t. \tag{11}$$

2.3 Finite-strain viscoelasticity

To introduce time dependency of the material behavior, the concept of free energy is used. The development of Simo (1987) for derivation of stress-strain relationships is being followed here. The split of the free-energy function $\Psi(\mathbf{E}, \mathbf{S}_{neq})$ is postulated to be

$$\Psi(\mathbf{E}, \mathbf{S}_{neq}) = U^0(J) + \overline{\Psi}^0\left(\overline{\mathbf{E}}\right) - \mathbf{S}_{neq} : \overline{\mathbf{E}} + \Psi_l(\mathbf{S}_{neq}), \tag{12}$$

where $\mathbf{S}_{neq}$ is the nonequilibrium stress which serves as an internal variable, the functions U^0 and $\overline{\Psi}^0$ are the volumetric and deviatoric parts of the initial free energy function Ψ^0. The last function in Eq. 12, Ψ_l, can be determined from the condition of thermodynamic equilibrium. The initial free energy function, Ψ^0, is assumed to take the form of Eq. 7 in this work.

The damage is introduced into the viscoelastic model under the assumption that it affects only the elastic energy term

$$\Psi(\mathbf{E}, \mathbf{S}_{neq}, W_m) = \eta \cdot (W_m)\Psi^0(\mathbf{E}) - \mathbf{S}_{neq} : \mathbf{E} + \Psi_l(\mathbf{S}_{neq}). \tag{13}$$

The second Piola-Kirchhoff stress then becomes

$$\mathbf{S} = \eta(W_m) \cdot \frac{\partial \Psi^0(\mathbf{E})}{\partial \mathbf{E}} - \mathbf{S}_{neq}. \tag{14}$$

Considering linear evolution of the internal variable $\mathbf{S}_{neq}$

$$\dot{\mathbf{S}}_{neq} + \frac{1}{\tau}\mathbf{S}_{neq} = \frac{1-\delta}{\tau}\eta(W_m)\frac{\partial \Psi^0(\mathbf{E})}{\partial \mathbf{E}}, \tag{15}$$

with τ being the so-called relaxation time and δ a dimensionless coefficient, a convolutional model is obtained

$$\mathbf{S} = \int_0^t K(t-s)\frac{\mathrm{d}}{\mathrm{d}s}\left(\eta(W_m)\frac{\partial \Psi^0(\mathbf{E})}{\partial \mathbf{E}}\right)\mathrm{d}s, \tag{16}$$

where $K(t)$ is a relaxation function. Usually it is expressed in the form

$$K(t) = \delta_0 + \sum_{n=1}^{N} \delta_n e^{-t/\tau_n} \tag{17}$$

involving more values of relaxation times τ_n and coefficients δ_n, where the number of the viscoelastic terms, N, must be chosen according to the number of time scales that have to be modeled. Apart from the values of δ_n and τ_n all being positive, a natural requirement on the coefficients is that $\delta_0 + \delta_1 + \ldots + \delta_N = 1$. The first coefficient, δ_0, corresponds to the long term elastic modulus. A material with $\delta_0 = 0$ is a fluid.

3 Experiments

The tram wheel segments are made from a rubber based on synthetic isoprene and butadiene elastomers. Experimental samples had to be cut directly from the segments used in the wheels. The water jet cutter was used. The small size of the segments limited the specimens geometry. Therefore, the specimens' geometry could not be in complete agreement with published recommendations (see Brown (2006)) and the rubber could not be tested in the pure shear. Fig. 1 illustrates used

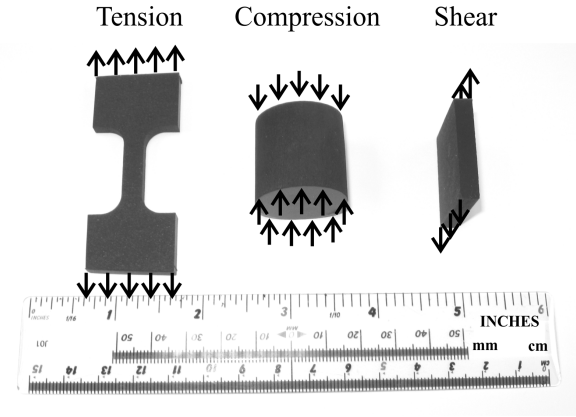

Figure 1: Experimental specimens.

shapes of the experimental specimens. Three types of tests were performed using Zwick/Roell Z050 testing machine: the tension, the compression and the simple shear test (see Fig. 2).

Major deformations of the real wheel segments are compressive and minor are shear. Predominantly, the segment strain magnitude is in the range from 10 to 15%. Maximum strain magnitude is 25%. Therefore, prescribed deformation progress during the experiments was as shown in Fig. 3, where $\varepsilon_1 = 0.15$, $\varepsilon_2 = 0.05$ and $\varepsilon_3 = 0.25$. The dwell was Δt_1 = 60 s. The strain rate between the dwells was $0.4\,\mathrm{min}^{-1}$ in all performed tests. The temperature influence was not analysed in this work, presented results were obtained in room temperature of 20 °C to 25 °C.

Unfortunately, the simple shear test was not successful. Adhesive bonded joints between the specimen and steel loading plates failed prior to achievement of the maximum strain. An example of obtained force-displacement curve is obvious from Fig. 10.

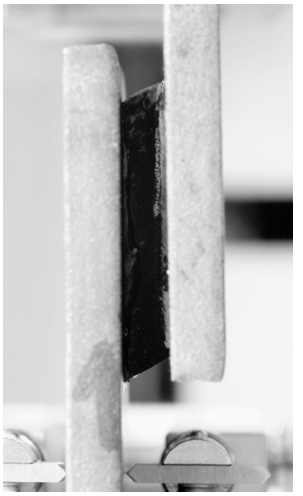

Figure 2: Simple shear test.

4 Solution of the state problems

As will be shown in section 5, a boundary value problem (BVP) has to be defined (and solved) for each experiment (tension, compression) in order to define the parameter identification problem. Solutions of the BVPs that were performed in this work are described below.

4.1 Uniaxial tension/compression

A state of uniform uniaxial strain can be assumed in the measured part of the tensile specimen. Therefore, the tensile test does not need to be simulated using the finite element method.

In the state of uniaxial tension/compression, the principal stretches are

$$\lambda_1 = \lambda, \quad \lambda_2 = \lambda_3 = \frac{1}{\sqrt{\lambda}} \tag{18}$$

and substitution into Eq. 8 yields the following formulas for strain energy density

$$W_{MR}(\lambda) = \sum_{ij} C_{ij} \left(\lambda^2 + \frac{2}{\lambda} - 3\right)^i \left(2\lambda + \frac{1}{\lambda^2} - 3\right)^j, \tag{19}$$

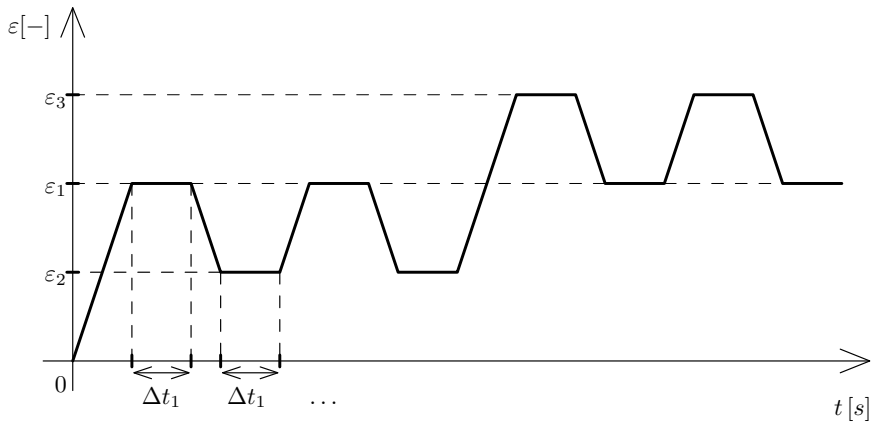

Figure 3: Prescribed deformation.

and true stress

$$\sigma_{MR}(\lambda) = \sum_{ij} C_{ij} \left(2\lambda + \frac{1}{\lambda^2} - 3\right)^{j-1} \left(\lambda^2 + \frac{2}{\lambda} - 3\right)^{i-1} \left(j\left(2 - \frac{2}{\lambda^3}\right)(\lambda^2 + \frac{2}{\lambda} - 3) + i\left(2\lambda - \frac{2}{\lambda^2}\right)\left(2\lambda + \frac{1}{\lambda^2} - 3\right)\right), \tag{20}$$

where the indices i, j correspond to the indices that appear in the Mooney-Rivlin model, namely $ij = 10$, 01, 11, 20, and 30.

The relations below have been derived by following the integration procedure described in Aba (2011):

$$\sigma_i = \eta(W_m^{(i)}) \cdot \sigma_{MR}^{(i)} - \sum_n \sigma_n^{(i)} \tag{21}$$

$$\sigma_n^{(i)} = \alpha_n^{(i)} \delta_n \sigma_{MR}^{(i)} + \beta_n^{(i)} \delta_n \left(\frac{\lambda^{(i)}}{\lambda^{(i-1)}}\right)^2 \sigma_{MR}^{(i-1)} + \gamma_n^{(i)} \left(\frac{\lambda^{(i)}}{\lambda^{(i-1)}}\right)^2 \sigma_n^{(i-1)} \tag{22}$$

$$\gamma_n^{(i)} = e^{-\Delta t_i/\tau_n} \tag{23}$$

$$\alpha_n^{(i)} = 1 - \frac{\tau_n}{\Delta t_i}(1 - \gamma_n^{(i)}) \tag{24}$$

$$\beta_n^{(i)} = \frac{\tau_n}{\Delta t_i}(1 - \gamma_n^{(i)}) - \gamma_n^{(i)} \tag{25}$$

with $\lambda^{(i)}$ being the value of prescribed stretch at i-th time level, t_i, $\sigma_{MR}^{(i)} = \sigma_{MR}(\lambda^{(i)})$ and $\Delta t_i = t_i - t_{i-1}$.

4.2 Finite-element simulations of compression and shear

The strain distribution in a compression specimen is not uniform (see Fig. 4) because it is not possible to fully avoid the friction between the specimen and the loading plates. The strain distribution in the shear specimen is also influenced, in this case, by adhesively bonded loading plates (see Fig. 5). Therefore, the compression and shear tests were simulated using the finite element method (FEM) in Abaqus 6.11 software.

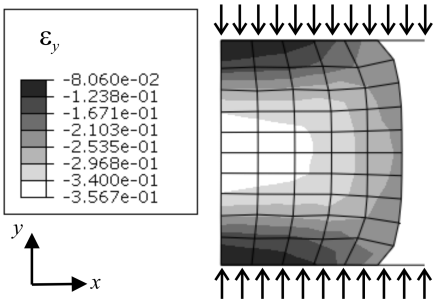

Figure 4: Distribution of normal strain in loading direction in case of compression test simulation.

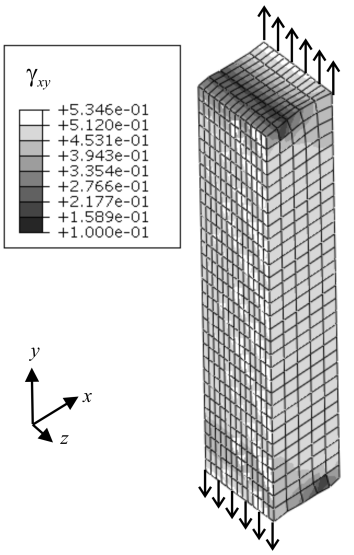

Figure 5: Distribution of engineering shear strain in *xy* plane in case of shear test simulation.

The compression and shear tests were simulated using first-order axisymmetric quadrilateral elements (see Fig. 4) and brick elements (see Fig. 5), respectively. The friction coefficient between the compression sample and the plates (modeled as rigid surfaces in a contact) was assumed 0.4. One symmetry plane was considered (*xy* plane in Fig. 5) in the shear simulation.

5 The identification problem

In the case of material parameters identification, a specimen is usually loaded with a prescribed displacement (deformation) or force and during the test both force and displacement at selected locations of the specimen are measured. The identification procedure usually consists of the following steps: Construct a state problem where only some of the measured quantities (displacement for instance) are used to define boundary conditions. From the solution of this *state problem* another quantities can be computed that can be compared to the other set of measured values. The difference between the measured and computed values defines a objective function to be minimized.

The most common way to define this function, which is also used in this work, is the least squares approach. Let us consider a system the state of which at a time step $t^{(i)}$ is described by a vector $y^{(i)}$. The measured quantity and its computed counterpart are denoted $\overline{\varphi}_i$ and $\varphi(\mathbf{x}, y^{(i)})$ respectively, where $\mathbf{x}$ denotes the vector of material parameters. The objective function that measures the difference between the model and the experiment is then defined as

$$F_1(\mathbf{x}) = \sum_{i \in I} \left(\overline{\varphi}_i - \varphi(\mathbf{x}, y^{(i)}) \right)^2, \tag{26}$$

where the set I is a set of all time steps in which the quantity $\overline{\varphi}_i$ has been measured.

As mentioned above, three experiments have been performed in different modes of loading: uniaxial tension, uniaxial compression, and simple shear (see section 3 for details). The shear loading mode was not used in the identification because of significantly higher requirement on FEM computational time and the shear experiment failure mentioned above. The shear simulation response was used only for the validation of the identified parameters. The tensile and compressive loading modes mean two different state problems and two different sets of measured data $\overline{\varphi}_i$ that must together lead to a single set of material parameters $\mathbf{x}$. To account for this, the objective function Eq. 26 has been modified as follows:

$$F_2(\mathbf{x}) = \frac{\sum_{i \in I} \left(\overline{\varphi}_i^t - \varphi^t(\mathbf{x}, y^{(i)}) \right)^2}{\sum_{i \in I} \left(\overline{\varphi}_i^t \right)^2} + \frac{\sum_{i \in I} \left(\overline{\varphi}_i^c - \varphi^c(\mathbf{x}, y^{(i)}) \right)^2}{\sum_{i \in I} \left(\overline{\varphi}_i^c \right)^2}. \tag{27}$$

The upper index t or c denotes either value corresponding either to the tension or the compression experiment/model. The sums in denominators have been introduced to compensate for the difference of magnitude of response in tension and compression. In this work, the response in tension were calculated analytically as $\varphi_i^t = \sigma_i$ using Eq. 21 and the response in compression is the force computed by the finite element method.

A general formulation of the identification problem is then

$$\begin{aligned} &\min_{\mathbf{x}} F_2(\mathbf{x}) \\ &s.t.\, \mathbf{h}(\mathbf{x}) \leq \mathbf{0} \end{aligned} \tag{28}$$

where the constraints represent requirements on the model's parameters imposed mostly by physical admissibility. These constraints are

$$r: \quad h_1(\mathbf{x}) = 1 - r \leq 0, \tag{29}$$

$$m: \quad h_2(\mathbf{x}) = -m \leq 0, \tag{30}$$

$$\beta: \quad h_3(\mathbf{x}) = -\beta \leq 0, \tag{31}$$

$$\delta_n: \quad h_{2+2n}(\mathbf{x}) = -\delta_n \leq 0, \tag{32}$$

$$\tau_n: \quad h_{3+2n}(\mathbf{x}) = -\tau_n \leq 0. \tag{33}$$

Only in the case of the first two Mooney-Rivlin parameters, C_{10} and C_{01}, there was an additional constraint in the form $0.9E \leq 6\,(C_{10} + C_{01}) \leq 2E$

$$C_{10}, C_{01}: \quad h_{3+2N}(\mathbf{x}) = 0.9E - 6\,(C_{10} + C_{01}) \leq 0, \tag{34}$$

$$h_{4+2N}(\mathbf{x}) = 6\,(C_{10} + C_{01}) - 2E \leq 0, \tag{35}$$

with the constant E being Young's modulus at infinitesimal strains. Here the relationship $E = 6\,(C_{10} + C_{01})$, which holds for the Mooney-Rivlin material, has been used.

5.1 Method for parameter identification

Considering that in the Ogden-Roxburgh model (OR), the damage does not evolve when $W_m = W_0$, we can identify the Mooney-Rivlin (MR) hyperelastic parameters (C_{ij}) first (considering only the first-loading parts of data). The parameters of the OR model (r, m, β) can be identified independently afterwards considering, similarly, only the reloading paths. Incorporating also the unloading paths would lead to local minima in the identification problem since the elastic response predicted by the model becomes attracted either to the loading or the unloading curve (Fig. 6) which differ in the real material's response due to viscoelastic effects.

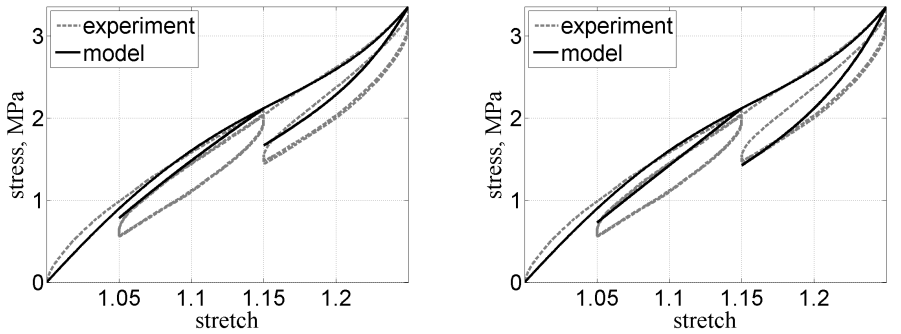

Figure 6: Examples of stress-stretch curves for two different local minima when optimizing parameters of Ogden-Roxburgh model.

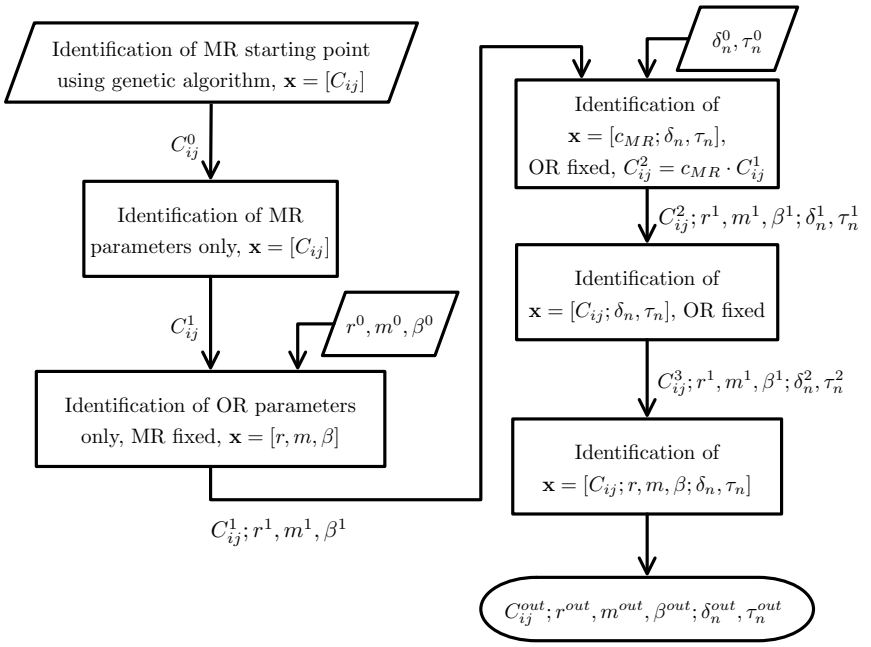

Figure 7: Block diagram of the identification process.

The identification of the viscoelastic parameters (δ_n, τ_n), however, cannot be performed without adjusting at least the Mooney-Rivlin parameters because viscoelasticity affects the response of the material in every time step. This part of the identification has been divided into three steps:

1. The vector of optimization variables is $\mathbf{x} = [c_{MR};\ \delta_n,\ \tau_n]$. The parameter c_{MR} serves for roughly adjusting the overall stiffness by multiplying the Mooney-Rivlin parameters that have been identified earlier.

2. Treating all Mooney-Rivlin parameters as separate optimization variables in addition to the viscoelasticity parameters, $\mathbf{x} = [C_{ij};\ \delta_n,\ \tau_n]$.

3. All previous successive steps lead to the final optimization of all parameters, $\mathbf{x} = [C_{ij};\ r,\ m,\ \beta;\ \delta_n,\ \tau_n]$ (see Fig. 7).

The starting point for the identification of Mooney-Rivlin parameters were obtained by a genetic algorithm in OptiSLang software. All other minimizations were carried out using the interior-point algorithm that is part of the Matlab Optimization Toolbox, although other algorithms were also tested during the early stages of the work. Namely SQP (Sequential Quadratic Programming), which also provided good results and seemed to be comparable in computation cost, and a simple gradient method, which was too demanding in the number of objective function evaluations.

6 Identification results

Using the procedure described in section 5.1, a set of parameters has been obtained. Their values are shown in Tab. 1 together with corresponding starting values.

Table 1: The identified values of material parameters.

parameter		starting point	identified value
C_{10}	kPa	2242	3753
C_{01}	kPa	1091	4506
C_{11}	kPa	−4326	−5558
C_{20}	kPa	301	463
C_{30}	kPa	10227	11080
r	-	1.5	1.873
m	MJ	1.0	1.000
β	-	0	0.201
δ_1	-	0.10	0.315
τ_{C1}	s	1.00	1.931
δ_2	-	0.05	0.136
τ_{C2}	s	10.00	10.125

Fig. 8 shows the comparison of stress-strain curves of the model and experiment in tension.

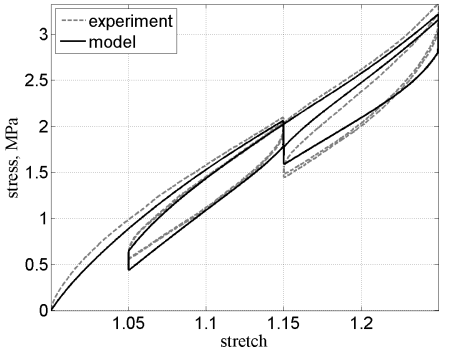

Figure 8: Stress-stretch curve of tensile test.

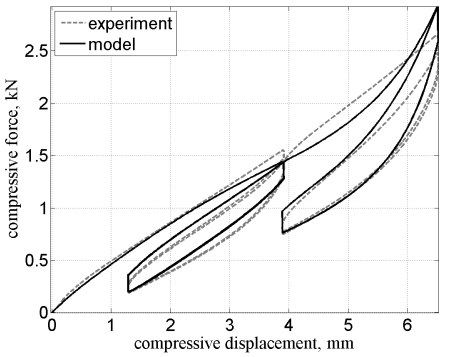

Figure 9: Force-displacement curve of compression test.

Similarly, Fig. 9 and Fig. 10 depict the force–displacement curves for the cases of compression and simple shear. Recall that the parameters of the material model have been identified on basis of tension and compression experimental data and the simple shear model serves only for validation of the results here.

As opposed to tension and compression, the shear experiment exhibits stiffer behavior under first loading. This can be attributed to the technology of bonding the shear specimens to metal plates; the specimen becomes stiffer near the surfaces where glue has been applied. The finite-element model did not account for this effect.

From the model response in compression and shear (see Fig. 9 and Fig. 10) a significant increase of stiffness is obvious at strain values close to maximum. Therefore maximum operational deformations have to be known prior to the identification to

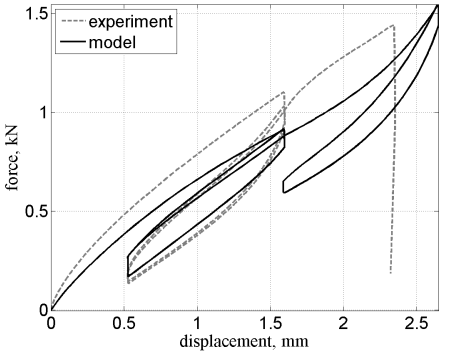

Figure 10: Force-displacement curve of shear test.

ensure that the investigated strain range is wider than the operational strain range. If there are any uncertainties about the operational strain range, the objective function should be adjusted to include final tangent of the model response.

7 Conclusion

In this work, a material model capable of describing dominant mechanical properties of the analyzed rubber has been composed. The rubber is used as a damping element in tram wheels. Applicable method of the identification of parameters of the material model was proposed. The comparison of numerical simulations and all experiments was in sufficient agreement although the simple shear test was not used directly in the identification process.

The selected model is suitable for quasistatic analysis which is satisfactory for present requirements of the rubber sprung wheels producer. Future work will focus on: (i) investigation of cyclic behavior of this type of material at broader range of strain rates and time scales and (ii) on analyzing of material model that could account for plasticity or permanent set.

Acknowledgement: This work was supported by the European Regional Development Fund (ERDF), project NTIS - New Technologies for Information Society, European Centre of Excellence, CZ.1.05/1.1.00/02.0090.

References

Bergström, J.; Boyce, M. (1998): Constitutive modeling of the large strain time-dependent behavior of elastomers. *Journal of the Mechanics and Physics of Solids*,

vol. 46, no. 5, pp. 931–954.

Bouasse, H.; Carrière, Z. (1903): Sur les courbes de traction du caoutchouc vulcanisé. *Annales de la faculté des sciences de Toulouse*, vol. 5, no. 3, pp. 257–283.

Brown, R. (2006): *Physical Testing of Rubber*. Springer.

Dassault Systèmes. *Abaqus 6.11 Theory Manual*, 2011.

Gent, A. N. (1996): A new constitutive relation for rubber. *Rubber Chemistry and Technology*, vol. 69, no. 1, pp. 59–61.

Govindjee, S.; Simo, J. (1991): A micro-mechanically based continuum damage model for carbon black-filled rubbers incorporating mullins' effect. *J. Mech. Phys. Solids*, vol. 39, no. 1, pp. 87–112.

Govindjee, S.; Simo, J. (1992): Transition from micro-mechanics to computationally efficient phenomenology: Carbon black filled rubbers incorporating mullins' effect. *J. Mech. Phys. Solids*, vol. 40, no. 1, pp. 213–233.

Holt, W. L. (1932): Behavior of rubber under repeated stresses. *Rubber Chemistry and Technology*, vol. 5, no. 1, pp. 79–89.

Lévesque, M.; Derrien, K.; Baptiste, D.; Gilchrist, M. D. (2008): On the development and parameter identification of schapery-type constitutive theories. *Mech Time-Depend Matter*, vol. 12, pp. 95–127.

Mullins, L. (1948): Effect of stretching on the properties of rubber. *Rubber Chemistry and Technology*.

Mullins, L. (1969): Softening of rubber by deformation. *Rubber Chemistry and Technology*, vol. 42, no. 1, pp. 339–362.

Mullins, L.; Tobin, N. R. (1957): Theoretical model for the elastic behavior of filler-reinforced vulcanized rubbers. *Rubber Chemistry and Technology*, vol. 30, no. 2, pp. 555–571.

Ogden, R. W.; Roxburgh, D. G. (1999): A pseudo-elastic model for the Mullins effect in filled rubber. *Proc. R. Soc. Lond. A*, , no. 455, pp. 2861–2877.

Qi, H.; Boyce, M. (2004): Constitutive model for stretch-induced softening of the stress-stretch behavior of elastomeric materials. *Journal of the Mechanics and Physics of Solids*, vol. 52, pp. 2187–2205.

Reese, S.; Govindjee, S. (1998): A theory of finite viscoelasticity and numerical aspects. *Int. J. Solids Structures*, vol. 35, no. 26–27, pp. 3455–3482.

Schapery, R. (1966): A theory of nonlinear thermoviscoelasticity based on irreversible thermodynamics. In *Proceedings of the 5th U.S. National Congress on Applied Mechanic*. ASME.

Simo, J. C. (1987): On a fully three-dimensional finite-strain viscoelastic damage model: Formulation and computational aspects. *Computer Methods in Applied Mechanics and Engineering*, vol. 60, pp. 153–173.